Degradable ZnS-supported bioorthogonal nanozymes with enhanced catalytic activity for intracellular activation of therapeutics

Xianzhi Zhang[1, ‡], Shichao Lin[1, 2, 3 ‡], Rui Huang[1], Aarohi Gupta[1], Stefano Fedeli[1], Roberto Cao-Milán[1], David C. Luther[1], Yuanchang Liu[1], Mingdi Jiang[1], Gengtan Li[1], Brayan Rondon[1], Hui Wei[2] and Vincent M. Rotello[1,*]

[1] Department of Chemistry, University of Massachusetts Amherst, 710 N. Pleasant St., Amherst, MA 01003, USA.

[2] Department of Biomedical Engineering, College of Engineering and Applied Sciences, Nanjing National Laboratory of Microstructures, Jiangsu Key Laboratory of Artificial Functional Materials, Nanjing University, Nanjing, Jiangsu 210023, People's Republic of China.

State Key Laboratory of Analytical Chemistry for Life Science, School of Chemistry and Chemical Engineering, Chemistry and Biomedicine Innovation Center (ChemBIC), Nanjing University, Nanjing, Jiangsu 210023, People's Republic of China.

[3] Current address: MOE Key Laboratory of Spectrochemical Analysis and Instrumentation, Key Laboratory for Chemical Biology of Fujian Province, Department of Chemical Biology, College of Chemistry and Chemical Engineering, Xiamen University, Xiamen 361005, China.

‡ X.Z. and S.L. contributed equally.

Abstract

Bioorthogonal catalysis using transition metal catalysts (TMCs) provides a toolkit for the *in situ* generation of imaging and therapeutic agents in biological environments. Integrating TMCs with nanomaterials mimics key properties of natural enzymes, providing bioorthogonal 'nanozymes'. ZnS nanoparticles provide a platform for bioorthogonal nanozymes using ruthenium catalysts embedded into self-assembled monolayers on the particle surface. These nanozymes uncage allylated pro-fluorophores and prodrugs. The ZnS core combines the non-toxicity and degradability with the enhancement of Ru catalysis through the release of thiolate surface ligands that accelerate the rate-determining step in the Ru-mediated deallylation catalytic cycle. The maximum rate of reaction (V_{max}) increases ~2.5 fold as compared to the non-degradable gold nanoparticle analog. The therapeutic potential of these bioorthogonal nanozymes is demonstrated by activating a chemotherapy drug from an inactive prodrug with the efficient killing of cancer cells.

Keywords: Bioorthogonal, nanozymes, degradation, catalysis, in situ drug activation

Introduction

Bioorthogonal chemistry uses abiotic chemical reactions as tools for biological and biomedical applications.[1-4] Bioorthogonal catalysis *via* transition metal catalysts (TMCs) provides *in situ* continuous generation of imaging and therapeutic agents using transformations that cannot be accomplished by natural enzymes.[5-9] However, the direct use of "naked" TMCs faces difficulties including poor water solubility, low stability, and lack of biocompatibility.[10,11] In particular, TMCs are generally very sensitive to the presence of serum proteins, limiting their utility in biological and biomedical applications.[12,13] Incorporating TMCs into nanomaterials provides bioorthogonal 'nanozymes' that feature enhanced solubility, stability, and biocompatibility.[14-18] The resulting nanozymes can activate therapeutics and imaging agents *in situ* from inactive precursors, providing on-demand "drug factories" for therapeutic applications including anti-cancer,[19-27] antimicrobial,[28,29] and anti-inflammatory treatments.[30]

Non-degradable nanomaterials, including gold nanoparticles[11-14, 29, 31, 32] and polystyrene microparticles.[19, 23,33-39] are commonly used as supports for bioorthogonal nanozymes. The lack of biodegradability of these scaffolds raises concerns for bioaccumulation and long-term toxicity.[40] Degradable scaffolds have the potential to increase the ultimate biocompatibility of nanozymes. As an example, Weissleder and Miller *et al.* used biodegradable poly(lactic-co-glycolic acid) (PLGA) polymeric nanoparticles to encapsulate palladium (Pd) catalysts and established anticancer therapy through activation of prodrugs.[26, 27]

Inorganic nanomaterials offer versatile platforms for bioorthogonal nanozymes, with control of structure and properties provided through engineering of the surface functionalization.[41] Zinc-based nanoparticles are feature biodegradability and high biocompatibility.[42] We report here the use of zinc sulfide nanoparticles (**ZnS_NP**) to formulate nanozymes (**ZnS_NZ**) through the encapsulation of ruthenium TMCs[13, 43] inside the monolayer (Figure 1a). Significantly, the degradation process enhanced bioorthogonal catalysis in solution and in cells by the release of thiolate surface ligands (Figure 1b, c). The therapeutic potential of **ZnS_NZ** was demonstrated by the activation of mitoxantrone, an anticancer drug. **ZnS_NZ** provided more efficient eradication of cancer cells compared to comparable gold nanoparticle-based nanozymes (**Au_NZ**) at similar catalyst levels. Taken together, this study demonstrated the integration of biocompatible degradable nanozymes with enhanced bioorthogonal catalysis through mechanism-based acceleration of catalysis *via* controlled nanoparticle degradation.

Results and discussion

ZnS_NP and **Au_NP** nanozymes were fabricated with a core diameter ~15 nm (Figure S1, supporting information for NP fabrication) and functionalized with identical cationic ligands. The resulting surface monolayer ligand features three crucial components: 1) a hydrophobic aliphatic chain to stabilize nanoparticles and encapsulate catalysts; 2) tetra(ethylene glycol) spacer to provide biocompatibility; and 3) a quaternary ammonium headgroup for enhanced water solubility and cell penetration (Figure 1a, Figure S2-3).

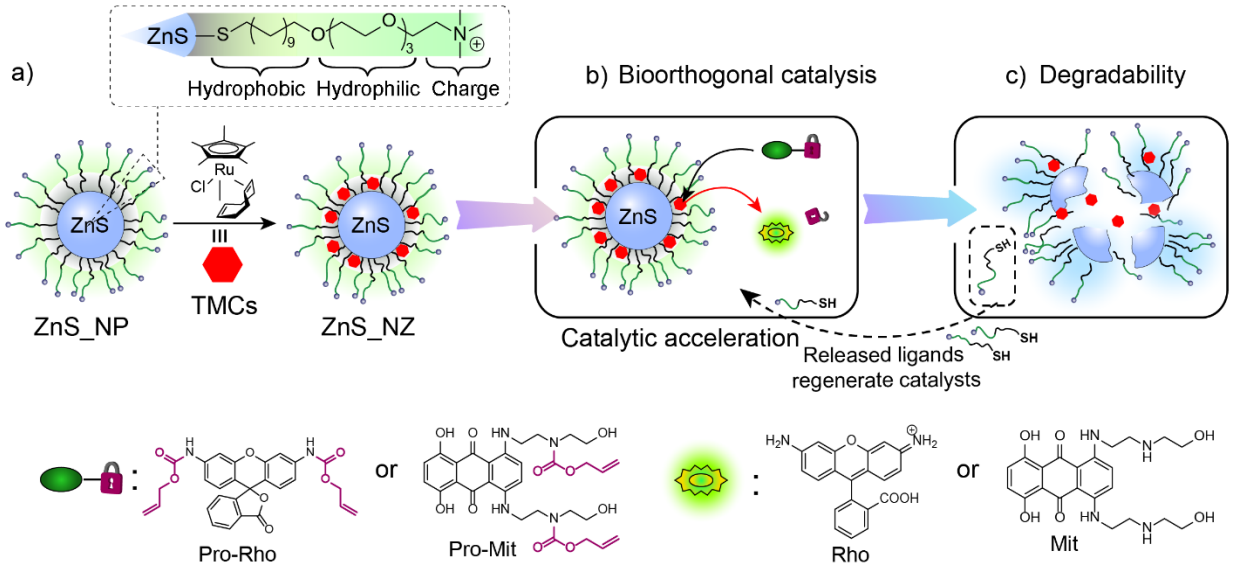

Figure 1. Schematic presentation of (a) generation of zinc sulfide nanozymes (**ZnS_NZ**) from zinc sulfide nanoparticles (**ZnS_NP**) and structures of substrates (**pro-Rho** and **pro-Mit**) and products (**Rho** and **Mit**), (b) the catalytic acceleration of **ZnS_NZ**, and (c) degradability of zinc sulfide platform.

The degradability of nanoparticles was quantified through changes in optical spectra and size distribution. **ZnS_NP** and **Au_NP** were incubated in deionized water at 37°C in the dark for 5 days. As shown in Figure 2a, a ~20% decrease in fluorescence was observed for **ZnS_NP**, suggesting the degradation of **ZnS_NP**. **Au_NP**, however, did not degrade under the same conditions, as evidenced by the negligible change in the surface plasmon resonance (SPR) band (Figure 2b). The size distributions of **ZnS_NP** and **Au_NP** before and after the incubation were consistent with the optical spectra (Figure 2c and d). The size distribution of **ZnS_NP** changed from monomodal to bimodal (Figure 2c), indicating small particles were generated during the degradation, followed by the formation of agglomerates *via* flocculation and coalescence processes. In contrast, **Au_NP** exhibited minimal changes in particle size and size distribution

(Figure 2d), demonstrating particle stability. research suggests that the presence of oxidants leads to the dissolution of ZnS.[44] We then incubated **ZnS_NP** under a nitrogen atmosphere and with hydrogen peroxide, respectively. As expected, **ZnS_NP** in a nitrogen environment had minimal size change, while **ZnS_NP** incubated with hydrogen peroxide degraded significantly (Figure S4).

We hypothesized that the changes in **ZnS_NP** size were first induced by the detachment of surface ligands. The release of thiolate surface ligands was tracked using Ellman's reagent (5,5'-dithiobis-(2-nitrobenzoic acid), **DTNB**). In the presence of free thiols, **DTNB** reacts with thiols to generate a yellow-colored product. Both **ZnS_NP** and **Au_NP** (20 nM) were mixed with 0.1 mM **DTNB**, and the absorbance was measured at 412 nm. A continuous increase of absorbance was observed for **ZnS_NP + DTNB**, while almost constant absorbance was found in the control groups (Figure 2e). The release of ligands from **ZnS_NP** was further studied using electrospray ionization mass spectrometry (ESI-MS). **ZnS_NP** was incubated in deionized water at 37°C for 3 days and the resulting solution was lyophilized and resuspended in methanol for ESI-MS. A peak representing oxidized ligands (disulfides) was observed (Figure S5), verifying the release of surface ligands during the degradation of **ZnS_NP**.

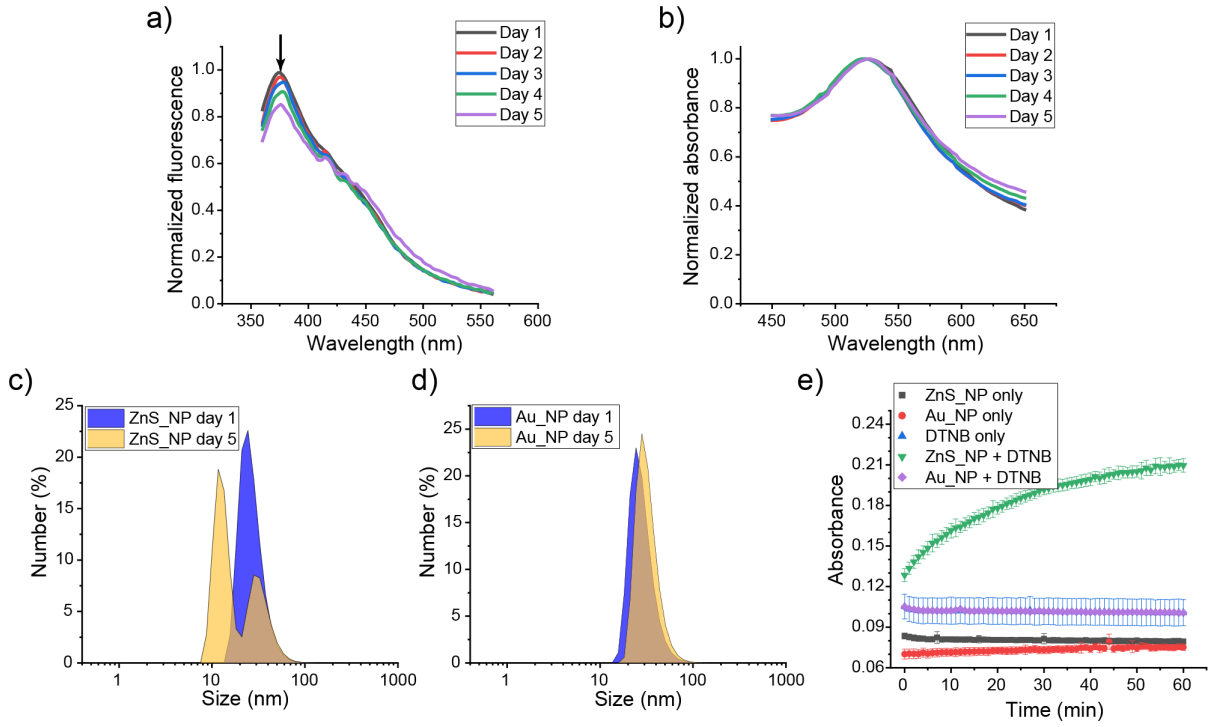

Figure 2. (a) Normalized fluorescence of 100 nM **ZnS_NP** in deionized water at 37°C in dark (λ_{ex}=265 nm, λ_{em}=360-560 nm). The decrease in fluorescence indicates the degradation of **ZnS_NP**. (b) Normalized absorbance spectra of 20 nM AuNP in deionized water at 37°C in dark indicating minimal degradation. (c) and (d) Size distribution of **ZnS_NP** (c) and **Au_NP** (d) before and after incubation for five days. (e) Absorbance at 412 nm of nanoparticles (20nM) reacted with 0.1 mM Ellman's reagent (**DTNB**). The increased absorbance of **ZnS_NP + DTNB** mirrored the release of thiolate ligands (Figure S5) during the degradation. N=3, mean ± SD shown.

Bioorthogonal nanozymes were generated by encapsulating a ruthenium-based transition metal catalyst [Cp*Ru(cod)Cl] (Cp* = pentamethylcyclopentadienyl, cod = 1,5-cyclooctadiene) into the monolayers of **ZnS_NP** and **Au_NP** to generate **ZnS_NZ** and **Au_NZ**, respectively. The encapsulation of the Ru catalyst for both nanozymes was quantified by inductively coupled plasma mass spectrometry (ICP-MS), with 1300 ± 100 catalyst molecules per **ZnS_NZ** and 1400 ± 200 Ru per **Au_NZ** (Supporting Table 1). The TEM and DLS (Figure S6-7) confirmed **ZnS_NZ** and **Au_NZ** did not show any aggregation after encapsulation. The release of catalysts from nanozymes in water was tracked for 5 days. **Au_NZ** had the negligible release of the catalyst, while **ZnS_NZ**, surprisingly, released less than 2% of the total catalyst (Figure S8).

The catalytic activity of nanozymes was quantified by the uncaging of Rhodamine-based pro-dye **pro_Rho** (synthesis in supporting information, Figure S9-10). Ruthenium catalysts specifically cleave the allyloxycarbonyl groups of **pro-Rho**,[43] with fluorogenesis allowing quantification of the catalytic activity of the nanozymes from the calibration curve of rhodamine

(Figure S11). As shown in Figure 3a, fluorescence increased after mixing nanozymes (5 nM) with **pro-Rho** (10 μM), indicating both **ZnS_NZ** and **Au_NZ** were active. Notably, **ZnS_NZ** showed ~2.5-fold enhancement in fluorescence relative to **Au_NZ**. Significantly, physiological oxidant level had negligible influence on the catalytic activity of nanozymes (Figure S12). The same enhancement was also exhibited for the V_{max} value (0.54 nM/min for **ZnS_NZ** and 0.22 nM/min for **Au_NZ**) and k_{cat} value (0.11/min and 0.044/min for **ZnS_NZ** and **Au_NZ**, respectively) from the Michaelis-Menten kinetic model (Figure 3b and c). Moreover, K_m increased ~2-fold for **ZnS_NZ** relative to **Au_NZ**.

We next probed the mechanistic origin for the increase in catalytic efficiency of **ZnS_NZ** relative to **Au_NZ**. Meggers *et al.* reported that the transfer of the allyl group from Ru catalysts to nucleophiles is the rate-determining step in the deallylation catalytic cycle (Figure 3d).[45] Therefore, good nucleophiles (including thiols) enhance the rate of this step, and hence the overall catalytic efficiency of uncaging.[46] Based on these findings, we hypothesized that the acceleration of **ZnS_NZ** was due to the release of thiolate ligands during the ZnS degradation (Figure 3d). To support our hypothesis, we incubated **ZnS_NZ** with **pro-Rho** in PBS at 37°C for 48 h with continuous shaking. The mixture was then lyophilized and resuspended in methanol for ESI-MS. As shown in Figure 3e and Figure S13, the peak at 462 (m/z) indicates that the allyl group on the **pro-Rho** has transferred to the thiol ligand. Moreover, the peak representing the oxidized disulfide ligand (m/z 421) was not significantly presented, indicating that the detached thiol ligands were allylated. This result indicates that thiol ligands were released from ZnS and participated in the ruthenium catalytic cycle.

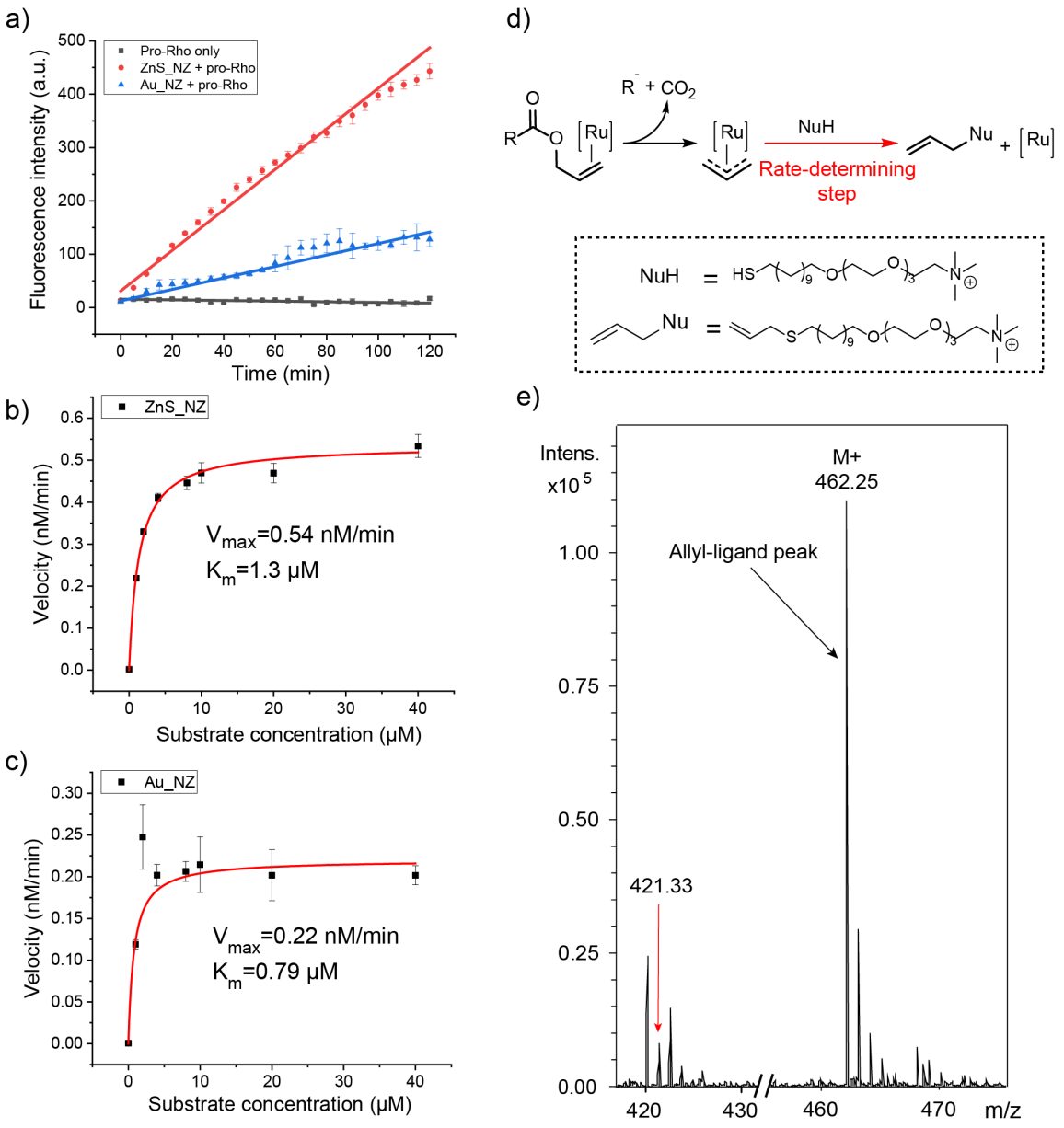

Figure 3. (a) Kinetic study of 5 nM nanozymes with 10 μM **pro-Rho** in PBS at 37 ºC. (b) and (c) The Michaelis–Menten kinetics of 5 nM nanozymes. **ZnS_NZ** showed ~2.5-fold enhancement in catalytic activity. Each data point represents the average of three replicates. Error bar stands for the standard deviation. (d) Proposed mechanism for deallylation reaction using the Ru catalyst. Thiols that were released from ZnS served as strong nucleophiles (Nu) and accelerated the rate-determining step of the catalytic cycle. (e) ESI-MS spectrum after **ZnS_NZ**-mediated decaging of **pro-Rho**. The free ligands (m/z 421) were converted to allylated ligand (m/z 462). The full spectrum is presented in Figure S13.

Having characterized the catalytic activity in solution, we investigated the ability of nanozymes to uncage **pro-Rho** in living cells. HeLa cells were incubated with different concentrations of **ZnS_NZ** and **Au_NZ** nanozymes in the culture medium for 24 h to evaluate

their cytotoxicity. Despite the same surface functionality and size, **Au_NZ** exhibited significantly higher toxicity than **ZnS_NZ** (Figure 4). Based on these toxicity data, a 5 nM nanozyme concentration was used for further cell studies. The cellular internalization of nanozymes was measured by tracking Ru using ICP-MS after 24 h incubation. **ZnS_NZ** showed slightly lower cellular levels than **Au_NZ**, possibly due to the degradation of **ZnS_NZ** (Figure S14). For the **pro-Rho** activation study, HeLa cells were treated with nanozymes for 24 h and washed with PBS to remove excess nanozymes. Fresh media containing **pro-Rho** (100 μM) was added to the cells for another 24 h, and the activation of **pro-Rho** in cells was imaged using confocal microscopy, with the intracellular fluorescence quantified using ImageJ software. As displayed in Figure 5a, cells treated with nanozymes exhibited green fluorescence while the negative control (**pro-Rho** only) showed a negligible signal. This result verified the ability of nanozyme' to perform bioorthogonal catalysis in cells. Importantly, **ZnS_NZ**-treated cells showed ~2.5-fold brighter fluorescence than **Au_NZ** from the confocal image (Figure 5a) and the quantification (Figure 5b). Flow cytometry analysis of fluorescence (>10,000 cells/condition) provided results consistent with the confocal data (Figure 5c), confirming the enhancement of catalysis in living cells by the ZnS nanoparticle scaffold.

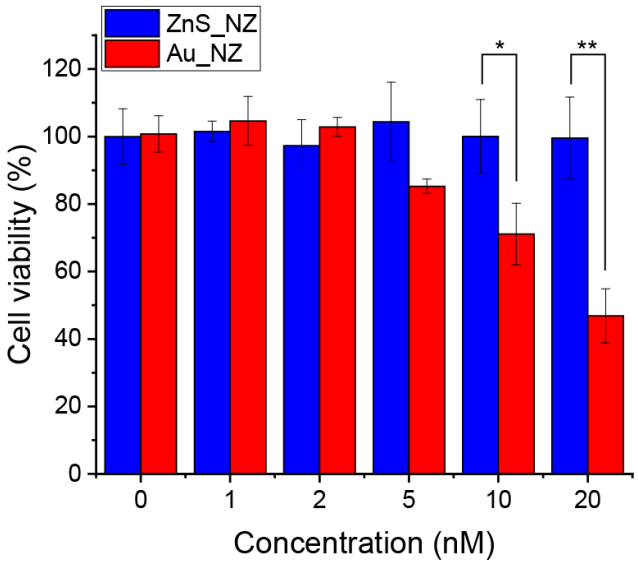

Figure 4. Cytotoxicity of **ZnS_NZ** and **Au_NZ**. **ZnS_NZ** exhibited significantly less toxicity than **Au_NZ**. Data are presented as mean ± standard deviation, n=3. *: 0.01<p<0.05; **: 0.001<p<0.01; ***: p<0.001.

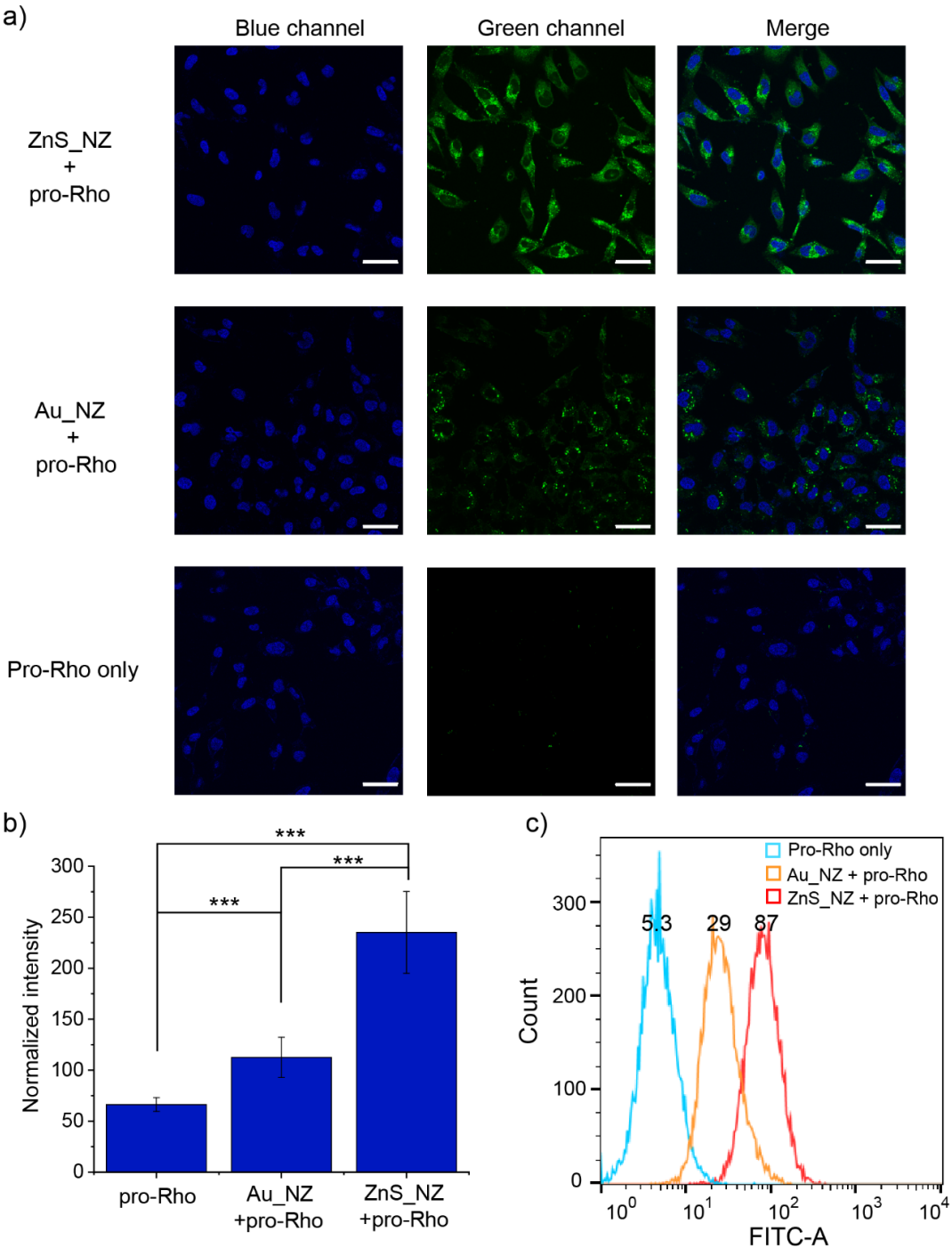

Figure 5. (a) Confocal images of HeLa cells incubated with nanozymes (5 nM) followed by the addition of **pro-Rho** (100 μM) for 24 h. The nucleus was stained by Hoechst 33342. Scale bar = 50 μm. (b) Quantification of intracellular fluorescence intensity by ImageJ software. Intracellular fluorescence from **ZnS_NZ** treated cells displayed ~2.5-fold higher intensity than **Au_NZ** treated ones. *: 0.01<p<0.05; **: 0.001<p<0.01; ***: p<0.001. (c) Flow cytometry of cells treated with **pro-Rho** only, **Au_NZ + pro-Rho**, and **ZnS_NZ + pro-Rho**. The means of three groups were 5.3, 29, 87 a.u., respectively.

We next explored the use of bioorthogonal **ZnS_NZ** for prodrug activation. A mitoxantrone (**Mit**) prodrug (**pro-Mit**) was used to evaluate the *in vitro* anticancer effect of nanozymes. The **pro-Mit** was synthesized by caging the pharmacophore of **Mit** with allyloxycarbonyl groups (synthesis in supporting information, Figure S15-16).[21] The toxicity of **pro-Mit** was reduced more than 20-fold compared to **Mit** (Figure S17). After incubation with nanozymes, **pro-Mit** was converted to active **Mit** (Figure 6a and Figure S18). HeLa cells were treated with nanozymes (5 nM) for 24 h followed **pro-Mit** (0-5 μM) for another 24 h. Compared with **pro-Mit** only, elevated toxicity was observed in the presence of nanozymes and **pro-Mit** (Figure 6b), emphasizing the effective killing of cancer cells. Significantly, **ZnS_NZ** induced better cancer cell eradication and apoptosis (Figure S19) than **Au_NZ** presumably because of the enhanced catalytic activity of **ZnS_NZ**.

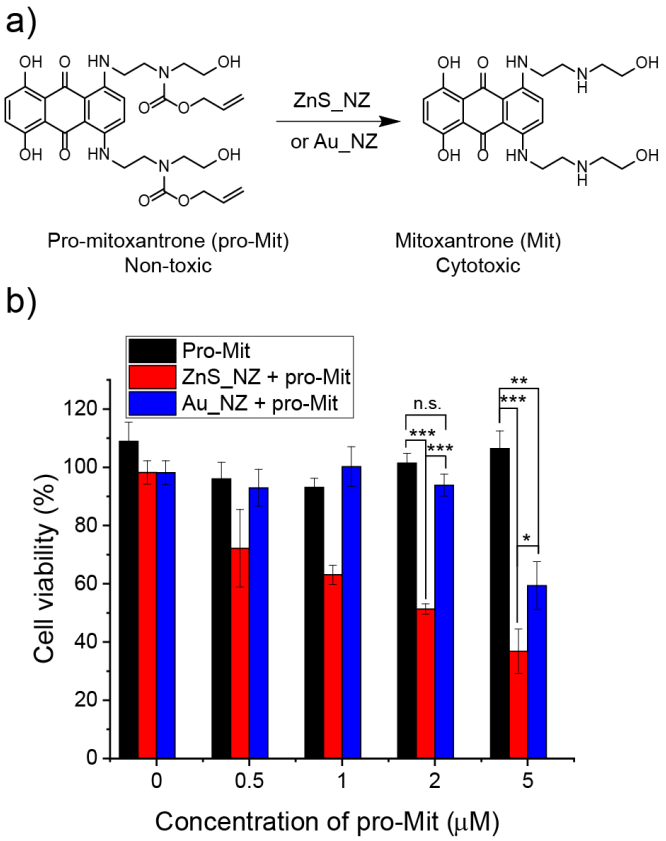

Figure 6. (a) Activation of prodrug (**pro-Mit**) by nanozymes. (b) Cell viability of HeLa cells incubated with 5 nM nanozymes followed by treatment with prodrug (24 h). The average cell viability was measured from three replicates, and the error bars represented the standard deviation. n.s.: 0.05<p; *: 0.01<p<0.05; **: 0.001<p<0.01; ***: p<0.001.

Conclusion

In summary, we have developed a strategy that uses surface functionalized ZnS nanoparticles for combined biodegradability and enhanced bioorthogonal catalysis through ligand-mediated acceleration of catalysis. In this process, released thiols serve as nucleophiles, accelerating the rate-determining step in the uncaging of allyl-caged molecules by Ru catalysts. As compared to other types of nanozymes (including FeS) that behave as enzyme mimics,[16,17,47-49] ZnS-supported nanozyme can employ chemical transformation that cannot be accomplished by natural enzymes. This study demonstrates that nano-scaffolds can actively participate in bioorthogonal catalysis as a cofactor rather than simply passively encapsulating the catalysts. The superior activity relative to non-degradable gold nanoparticle nanozymes was demonstrated through the fluorophore and drug release *in vitro*, underlining the significance for biomedical applications. Overall, ZnS nanozymes offer a biocompatible platform for the safe and efficient production of imaging and therapeutic agents *in situ*, promoting the clinical translation of bioorthogonal catalysis. Medical treatments featuring bioresorbable nanozymes can be safely implemented in living systems, providing localized therapies with minimal side effects. The biodegradability of the materials also avoids the risk of particle accumulation. Taken together, ZnS nanoparticles integrate biodegradability and enhanced catalytic activity, providing promising bioorthogonal nanozymes for biomedical applications.

Experimental section

Thiol detection

The release of thiols was detected by following the previous report using Ellman's reagent.[50,51] Briefly, DTNB was dissolved in 0.1 M phosphate buffer containing 1 mM EDTA to obtain the stock solution. Then, 100 µL solution containing 20 nM nanoparticles and 0.1mM DTNB was added into a 96-well clear plate and tracked the absorbance at 412 nm at 37°C using Molecular Devices SpectraMax M2 plate reader for 1 h.

Encapsulation of Ru into the monolayer of nanoparticles

Ruthenium catalyst (2mg) was dissolved in 0.5 mL acetone and added to an 8 mL aqueous solution of nanoparticles. The solution was applied with ultracentrifugation eight times to remove the excess catalysts to obtain the corresponding nanozymes.

Kinetic study of nanozymes

In a 96-well black plate, **pro-Rho** solution (10 μL, 100 μM) was added, followed by adding 90 μL nanozymes solution in PBS to make the final solution containing 10 μM **pro-Rho** and 5 nM nanozymes. **Pro-Rho** alone was used as the negative control. For Michaelis-Menten kinetic study, a solution containing nanozymes (5 nM) and **pro-Rho** (0, 1, 2, 4, 8, 10, 20, and 40 μM) was added in a 96-well black plate. The kinetic results were obtained by tracking the fluorescence (λ_{ex}: 488 nm, λ_{em}: 521 nm, cutoff: 515 nm) using a Molecular Devices SpectraMax M2 plate reader at 37°C for 2 h continuously.

Pro-Rho activation in living cells by nanozymes

HeLa cells were seeded at 150k in the confocal dish or 200k per well in a 6-well plate one night prior to the confocal imaging experiment or flow cytometry, respectively. Cells were treated with 5 nM **ZnS_NZ** or **Au_NZ** for 24 h, followed by multiply washings to remove the excess nanozymes. Then, fresh media containing 100 μM **pro-Rho** was incubated with cells for another 24 h. Cells were washed by PBS three times. For the confocal study, cells were stained using Hoechst 33342, washed by PBS, and imaged under Nikon A1 spectral detector confocal microscope (A1SP) using a 40x objective. For flow cytometry, cells were harvested and resuspended in PBS and analyzed using FACS LSR II (BD Biosciences). A total of 10,000 events per sample were analyzed.

Intracellular activation of pro-Mit

HeLa cells (7k) were seeded in a 96 well plate one day before the experiment. Nanozymes (5nM) were incubated with cells for 24 h followed by multiple washing by PBS. Fresh media containing various concentrations of **pro-Mit** (0-5 μM) was then added to the cells for another 24 h. **Pro-Mit** alone was used as the negative control. Cell viability was determined by Alamar Blue assay using the M2 microplate reader (λ_{ex} = 560 nm, λ_{em} = 590 nm).

Author information

Corresponding author

*E-mail: rotello@chem.umass.edu

Notes:

The authors declare no competing financial interest.

Acknowledgement

This work is supported by the National Institutes of Health EB022641 and the NSF (CHE- 2108044, ICP-MS) S. Lin thanks the financial support from Visiting Scholar Funding of Nanjing University.

Associated Content

Supporting Information

Electronic supporting information (ESI) is available free of charge at DOI: xxxx.

Materials; Synthesis, characterization of nanomaterials, pro-Rho, and pro-Mit; Toxicity of Mit and pro-Mit.

Reference

1 Sletten, E. M.; Bertozzi, C. R. Bioorthogonal Chemistry: Fishing for Selectivity in a Sea of Functionality. *Angew. Chemie Int. Ed.* **2009**, *48*, 6974–6998.

2 Prescher, J. A.; Bertozzi, C. R. Chemistry in Living Systems. *Nat. Chem. Biol.* **2005**, *1*, 13–21.

3 Wang, J.; Wang, X.; Fan, X.; Chen, P. R. Unleashing the Power of Bond Cleavage Chemistry in Living Systems. *ACS Cent. Sci.* **2021**, *7*, 929–943.

4 Bird, R. E.; Lemmel, S. A.; Yu, X.; Zhou, Q. A. Bioorthogonal Chemistry and Its Applications. *Bioconjug. Chem.* **2021**, *32*, 2457–2479.

5 Martínez-calvo, M.; Mascareñas, J. L. Organometallic Catalysis in Biological Media and Living Settings. *Coord. Chem. Rev.* **2018**, *359*, 57–79.

6 van de L'Isle, M. O. N.; Ortega-Liebana, M. C.; Unciti-Broceta, A. Transition Metal Catalysts for the Bioorthogonal Synthesis of Bioactive Agents. *Curr. Opin. Chem. Biol.* **2021**, *61*, 32–42.

7 Li, J.; Chen, P. R. Development and Application of Bond Cleavage Reactions in Bioorthogonal Chemistry. *Nat. Chem. Biol.* **2016**, *12*, 129–137.

8 Bai, Y.; Chen, J.; Zimmerman, S. C. Designed Transition Metal Catalysts for Intracellular Organic Synthesis. *Chem. Soc. Rev.* **2018**, *47*, 1811–1821.

9 Liu, Y.; Bai, Y. Design and Engineering of Metal Catalysts for Bio-Orthogonal Catalysis in Living Systems. *ACS Appl. Bio Mater.* **2020**, *3*, 4717–4746.

10 Zhang, X.; Huang, R.; Gopalakrishnan, S.; Cao-milán, R.; Rotello, V. M. Bioorthogonal Nanozymes : Progress towards Therapeutic Applications. *Trends Chem.* **2019**, *1*, 90–98.

11 Tonga, G. Y.; Jeong, Y.; Duncan, B.; Mizuhara, T.; Mout, R.; Das, R.; Kim, S. T.; Yeh, Y. C.; Yan, B.; Hou, S.; et al. Supramolecular Regulation of Bioorthogonal Catalysis in Cells Using Nanoparticle-Embedded Transition Metal Catalysts. *Nat. Chem.* **2015**, *7*, 597–603.
12 Zhang, X.; Liu, Y.; Gopalakrishnan, S.; Castellanos-Garcia, L.; Li, G.; Malassine, M.; Uddin, I.; Huang, R.; Luther, D. C.; Vachet, R. W.; et al. Intracellular Activation of Bioorthogonal Nanozymes through Endosomal Proteolysis of the Protein Corona. *ACS Nano* **2020**, *14*, 4767–4773.
13 Zhang, X.; Fedeli, S.; Gopalakrishnan, S.; Huang, R.; Gupta, A.; Luther, D. C.; Rotello, V. M. Protection and Isolation of Bioorthogonal Metal Catalysts by Using Monolayer-Coated Nanozymes. *ChemBioChem* **2020**, *21*, 2759–2763.
14 Cao-Milán, R.; He, L. D.; Shorkey, S.; Tonga, G. Y.; Wang, L. S.; Zhang, X.; Uddin, I.; Das, R.; Sulak, M.; Rotello, V. M. Modulating the Catalytic Activity of Enzyme-like Nanoparticles through Their Surface Functionalization. *Mol. Syst. Des. Eng.* **2017**, *2*, 624–628.
15 Wang, W.; Zhang, X.; Huang, R.; Hirschbiegel, C. M.; Wang, H.; Ding, Y.; Rotello, V. M. In Situ Activation of Therapeutics through Bioorthogonal Catalysis. *Adv. Drug Deliv. Rev.* **2021**, *176*, 113893
16 Wu, J.; Wang, X.; Wang, Q.; Lou, Z.; Li, S.; Zhu, Y.; Qin, L.; Wei, H. Nanomaterials with Enzyme-like Characteristics (Nanozymes): Next-Generation Artificial Enzymes (II). *Chem. Soc. Rev.* **2019**, *48*, 1004–1076.
17 Huang, Y.; Ren, J.; Qu, X. Nanozymes : Classification , Catalytic Mechanisms , Activity Regulation , and Applications. *Chem. Rev.* **2019**, *119*, 4357–4412.
18 Fedeli, S.; Im, J.; Gopalakrishnan, S.; Elia, J. L.; Gupta, A.; Kim, D.; Rotello, V. M. Nanomaterial-Based Bioorthogonal Nanozymes for Biological Applications. *Chem. Soc. Rev.* **2021**, *50*, 13467–13480
19 Weiss, J. T.; Dawson, J. C.; Macleod, K. G.; Rybski, W.; Fraser, C.; Torres-Sánchez, C.; Patton, E. E.; Bradley, M.; Carragher, N. O.; Unciti-Broceta, A. Extracellular Palladium-Catalysed Dealkylation of 5-Fluoro-1-Propargyl-Uracil as a Bioorthogonally Activated Prodrug Approach. *Nat. Commun.* **2014**, *5*, 3277.
20 Chen, Z.; Li, H.; Bian, Y.; Wang, Z.; Chen, G.; Zhang, X.; Miao, Y.; Wen, D.; Wang, J.; Wan, G.; et al. Bioorthogonal Catalytic Patch. *Nat. Nanotechnol.* **2021**, *16*, 933–941.
21 Zhang, X.; Landis, R. F.; Keshri, P.; Cao-Milán, R.; Luther, D. C.; Gopalakrishnan, S.; Liu, Y.; Huang, R.; Li, G.; Malassiné, M.; et al. Intracellular Activation of Anticancer Therapeutics Using Polymeric Bioorthogonal Nanocatalysts. *Adv. Healthc. Mater.* **2021**, *10*, 2001627.

22 Sancho-albero, M.; Rubio-ruiz, B.; Pérez-lópez, A. M.; Sebastián, V.; Martín-duque, P.; Arruebo, M.; Santamaría, J.; Unciti-broceta, A. Cancer-Derived Exosomes Loaded with Ultrathin Palladium Nanosheets for Targeted Bioorthogonal Catalysis. *Nat. Catal.* **2019**, *2*, 864–872.
23 Bray, T. L.; Salji, M.; Brombin, A.; Ana, M. P.; Galbraith, L. C. A.; Patton, E. E.; Leung, H. Y.; Unciti-Broceta, A. Bright Insights into Palladium-Triggered Local Chemotherapy. *Chem. Sci.* **2018**, *9*, 7354–7361.
24 Wang, F.; Zhang, Y.; Liu, Z.; Du, Z.; Zhang, L.; Ren, J.; Qu, X. A Biocompatible Heterogeneous MOF – Cu Catalyst for In Vivo Drug Synthesis in Targeted Subcellular Organelles. *Angew. Chemie* **2019**, *58*, 6987–6992.
25 Clavadetscher, J.; Indrigo, E.; Chankeshwara, S. V; Lilienkampf, A.; Bradley, M. In-Cell Dual Drug Synthesis by Cancer-Targeting Palladium Catalysts. *Angew. Chemie* **2017**, *129*, 6968–6972.
26 Miller, M. A.; Mikula, H.; Luthria, G.; Li, R.; Kronister, S.; Prytyskach, M.; Kohler, R. H.; Mitchison, T.; Weissleder, R. Modular Nanoparticulate Prodrug Design Enables Efficient Treatment of Solid Tumors Using Bioorthogonal Activation. *ACS Nano* **2018**, *12*, 12814–12826.
27 Miller, M. A.; Askevold, B.; Mikula, H.; Kohler, R. H.; Pirovich, D.; Weissleder, R. Nano-Palladium Is a Cellular Catalyst for in Vivo Chemistry. *Nat. Commun.* **2017**, *8*, 15906.
28 Huang, R.; Li, C.; Cao-milan, R.; He, L. D.; Makabenta, J. M.; Zhang, X.; Yu, E.; Rotello, V. M. Polymer-Based Bioorthogonal Nanocatalysts for the Treatment of Bacterial Biofilms. *J. Am. Chem. Soc.* **2020**, *142*, 10723–10729.
29 Cao-milan, R.; Gopalakrishnan, S.; He, L. D.; Huang, R.; Wang, L.; Castellanos, L.; Luther, D. C.; Landis, R. F.; Makabenta, J. M. V; Li, C.; et al. Thermally Gated Bio-Orthogonal Nanozymes with Supramolecularly Confined Porphyrin Catalysts for Antimicrobial Uses Thermally Gated Bio-Orthogonal Nanozymes with Supramolecularly Confined Porphyrin Catalysts for Antimicrobial Uses. *Chem* **2020**, *6*, 1–12.
30 Du, Z.; Liu, C.; Song, H.; Scott, P.; Liu, Z.; Ren, J.; Qu, X. Neutrophil-Membrane-Directed Bioorthogonal Synthesis of Inflammation-Targeting Chiral Drugs. *Chem* **2020**, *6*, 2060–2072.
31 Gupta, A.; Das, R.; Yesilbag Tonga, G.; Mizuhara, T.; Rotello, V. M. Charge-Switchable Nanozymes for Bioorthogonal Imaging of Biofilm-Associated Infections. *ACS Nano* **2018**, *12*, 89–94.
32 Das, R.; Landis, R. F.; Tonga, G. Y.; Cao-mila, R.; Luther, D. C.; Rotello, V. M. Control of Intra- versus Extracellular Bioorthogonal Catalysis Using Surface- Engineered Nanozymes. *ACS Nano* **2019**, *13*, 229–235.

33 Yusop, R. M.; Unciti-Broceta, A.; Johansson, E. M. V.; Sánchez-Martín, R. M.; Bradley, M. Palladium-Mediated Intracellular Chemistry. *Nat. Chem.* **2011**, *3*, 239–243.
34 Weiss, J. T.; Dawson, J. C.; Fraser, C.; Rybski, W.; Torres-Sánchez, C.; Bradley, M.; Patton, E. E.; Carragher, N. O.; Unciti-Broceta, A. Development and Bioorthogonal Activation of Palladium-Labile Prodrugs of Gemcitabine. *J. Med. Chem.* **2014**, *57*, 5395–5404.
35 Weiss, J. T.; Carragher, N. O.; Unciti-broceta, A. Palladium-Mediated Dealkylation of N-Propargyl-Floxuridine as a Bioorthogonal Oxygen-Independent Prodrug Strategy. *Sci. Rep.* **2015**, *5*, 9329.
36 Rubio-Ruiz, B.; Weiss, J. T.; Unciti-Broceta, A. Efficient Palladium-Triggered Release of Vorinostat from a Bioorthogonal Precursor. *J. Med. Chem.* **2016**, *59*, 9974–9980.
37 Pérez-López, A. M.; Rubio-Ruiz, B.; Sebastián, V.; Hamilton, L.; Adam, C.; Bray, T. L.; Irusta, S.; Brennan, P. M.; Lloyd-Jones, G. C.; Sieger, D.; et al. Gold-Triggered Uncaging Chemistry in Living Systems. *Angew. Chemie - Int. Ed.* **2017**, *56*, 12548–12552.
38 Clavadetscher, J.; Indrigo, E.; Chankeshwara, S. V.; Lilienkampf, A.; Bradley, M. In-Cell Dual Drug Synthesis by Cancer-Targeting Palladium Catalysts. *Angew. Chemie - Int. Ed.* **2017**, *56*, 6864–6868.
39 Adam, C.; Pérez-López, A. M.; Hamilton, L.; Rubio-Ruiz, B.; Bray, T. L.; Sieger, D.; Brennan, P. M.; Unciti-Broceta, A. Bioorthogonal Uncaging of the Active Metabolite of Irinotecan by Palladium-Functionalized Microdevices. *Chem. - A Eur. J.* **2018**, *24*, 16783–16790.
40 Luther, D. C.; Huang, R.; Jeon, T.; Zhang, X.; Lee, Y. W.; Nagaraj, H.; Rotello, V. M. Delivery of Drugs, Proteins, and Nucleic Acids Using Inorganic Nanoparticles. *Adv. Drug Deliv. Rev.* **2020**, *15*, 188–213.
41 Erathodiyil, N.; Ying, J. Y. Functionalization of Inorganic Nanoparticles for Bioimaging Applications. *Acc. Chem. Res.* **2011**, *44*, 925–935.
42 Dargusch, M. S. Acta Biomaterialia The Influence of Alloying and Fabrication Techniques on the Mechanical Properties , Biodegradability and Biocompatibility of Zinc : A Comprehensive Review. *Acta Biomater.* **2019**, *87*, 1–40.
43 Streu, C.; Meggers, E. Ruthenium-Induced Allylcarbamate Cleavage in Living Cells. *Angew. Chemie - Int. Ed.* **2006**, *45*, 5645–5648.
44 Eskelsen, J. R.; Xu, J.; Chiu, M.; Moon, J.; Wilkins, B.; Graham, D. E.; Gu, B.; Pierce, E. M. Influence of Structural Defects on Biomineralized ZnS Nanoparticle Dissolution: An in-Situ Electron Microscopy Study. *Environ. Sci. Technol.* **2018**, *52*, 1139–1149.
45 Völker, T.; Dempwolff, F.; Graumann, P. L.; Meggers, E. Progress towards Bioorthogonal Catalysis with Organometallic Compounds. *Angew. Chemie - Int. Ed.* **2014**, *53*, 10536–10540.

46 Völker, T.; Meggers, E. Chemical Activation in Blood Serum and Human Cell Culture: Improved Ruthenium Complex for Catalytic Uncaging of Alloc-Protected Amines. *ChemBioChem* **2017**, *18*, 1083–1086.

47 Kumar, S.; Kumar, A.; Biswas, P.; Srivastava, D. N.; Paul, P.; Mondal, A.; Adhikary, B. Synthesis and Characterization of FeS Nanoparticles Obtained from a Dithiocarboxylate Precursor Complex and Their Photocatalytic , Electrocatalytic and Biomimic Peroxidase Behavior. *Appl. Catal. A, Gen.* **2012**, *419–420*, 170–177.

48 Dutta, A. K.; Maji, S. K.; Srivastava, D. N.; Mondal, A.; Biswas, P.; Paul, P.; Adhikary, B. Synthesis of FeS and FeSe Nanoparticles from a Single Source Precursor: A Study of Their Photocatalytic Activity, Peroxidase-Like Behavior, and Electrochemical Sensing of H_2O_2. *ACS Appl. Mater. Interfaces* **2012**, *4*, 1919–1927.

49 Dai, Z.; Liu, S.; Bao, J.; Ju, H. Nanostructured FeS as a Mimic Peroxidase for Biocatalysis and Biosensing. *Chem. - A Eur. J.* **2009**, *15*, 4321–4326.

50 Sharma, S. K.; Adumeau, P.; Keinänen, O.; Sisodiya, V.; Sarvaiya, H.; Tchelepi, R.; Korsen, J. A.; Pourat, J.; Edwards, K. J.; Ragupathi, A.; et al. Synthesis and Comparative in Vivo Evaluation of Site-Specifically Labeled Radioimmunoconjugates for DLL3-Targeted ImmunoPET. *Bioconjug. Chem.* **2021**, *32*, 1255–1262.

51 Ellman, G. L. Tissue sulfhydryl groups. *Arch. Biochem. Biophys.* **1959**, *82*, 70– 77.

TOC Graphic